CHEMISTRY OF MATERIALS

Article

pubs.acs.org/cm

Enhanced Electrochemical Energy Storage by Nanoscopic Decoration of Endohedral and Exohedral Carbon with Vanadium Oxide via Atomic Layer Deposition

Simon Fleischmann,[†,‡] Nicolas Jäckel,[†,‡] Marco Zeiger,[†,‡] Benjamin Krüner,[†,‡] Ingrid Grobelsek,[†] Petr Formanek,[§] Soumyadip Choudhury,[†,§] Daniel Weingarth,[†] and Volker Presser*[,†,‡]

[†]INM - Leibniz Institute for New Materials, 66123 Saarbrücken, Germany

[‡]Department of Materials Science and Engineering, Saarland University, 66123 Saarbrücken, Germany

[§]Leibniz-Institut für Polymerforschung Dresden e. V., 01069 Dresden, Germany

Supporting Information

ABSTRACT: Atomic layer deposition (ALD) is a facile process to decorate carbon surfaces with redox-active nanolayers. This is a particularly attractive route to obtain hybrid electrode materials for high performance electrochemical energy storage applications. Using activated carbon and carbon onions as representatives of substrate materials with large internal or external surface area, respectively, we have studied the enhanced energy storage capacity of vanadium oxide coatings. While the internal porosity of activated carbon readily becomes blocked by obstructing nanopores, carbon onions enable the continued deposition of vanadia within their large interparticle voids. Electrochemical benchmarking in lithium perchlorate in acetonitrile (1 M $LiClO_4$) showed a maximum capacity of 122 mAh/g when using vanadia coated activated carbon and 129 mAh/g for vanadia coated carbon onions. There is an optimum amount of vanadia between 50 and 65 wt % for both substrates that results in an ideal balance between redox-activity and electrical conductivity of the hybrid electrode. Assembling asymmetric (charge balanced) full-cells, a maximum specific energy of 38 Wh/kg and 29 Wh/kg was found for carbon onions and activated carbon, respectively. The stability of both systems is promising, with a capacity retention of ~85−91% after 7000 cycles for full-cell measurements.

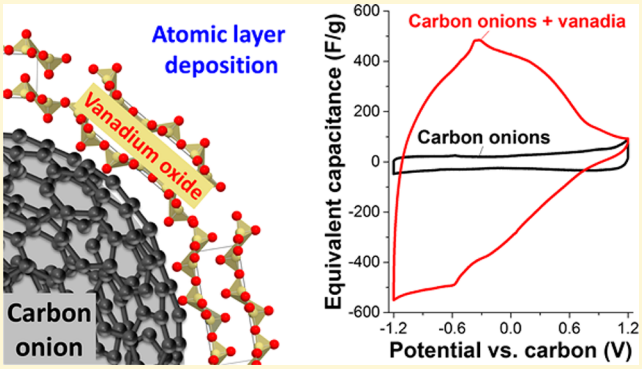

1. INTRODUCTION

Supercapacitors are devices for rapid and efficient electrochemical energy storage,[1] distinguished by high specific power, fast charge and discharge, and long lifetimes. However, supercapacitors suffer from an energy density significantly below state-of-the-art lithium-ion batteries, commonly by an order of magnitude.[2] The most common variety of supercapacitors, so-called electrical double-layer capacitors (EDLCs), store energy via reversible ion electrosorption at electrically charged fluid/solid interfaces of high surface area carbon electrodes.[3] So far, various carbons and carbon nanomaterials have been extensively studied including activated carbons (ACs),[4,5] carbon onions (or onion-like carbon, OLC),[6,7] carbon nanotubes,[8,9] graphene,[10,11] carbon nanofibers,[12,13] and carbon aerogels.[14] The most common group of electrode materials is ACs because of their low cost and high specific surface area (SSA), which can reach up to about 3000 m^2/g,[15,16] enabling specific double-layer capacitances of typically 100−200 F/g (equal to 33−66 mAh/g) in aqueous electrolytes.[2]

With a common diameter in the micrometer range, the high intraparticle porosity (inner porosity) of AC particles may reduce the high power performance of AC-based supercapacitors due to ion transport limitations.[17] Thus, materials with a large interparticle porosity (outer porosity originating from a nanoscopic primary particle size) are highly attractive, for example, carbon nanotubes, graphene, or carbon onions.[2,6,18] In particular, carbon onions have been found as promising candidates for high power supercapacitor electrodes. Structurally, carbon onions are small carbon quasi-nanospheres composed of concentrically stacked graphitic shells,[19] usually without inner porosity and surface area values in the range of 200−600 m^2/g.[20] A facile and scalable synthesis route for carbon onions is the thermal annealing of nanodiamond powders in inert atmosphere or vacuum.[21] During the annealing process, sp^3-hybridized nanodiamond is progressively converted to quasi-spherical sp^2-carbon onions, yielding

Received: February 20, 2016
Revised: March 27, 2016
Published: March 28, 2016

DOI: 10.1021/acs.chemmater.6b00738
Chem. Mater. 2016, 28, 2802−2813

particles of about 5−10 nm in diameter.[19] Given the moderate surface area (typically four-times smaller than activated carbon), carbon onions themselves only provide a specific capacitance of about 20−40 F/g (= 7−14 mAh/g) in aqueous electrolytes.[7] Yet, their electrical conductivity is about one order of magnitude higher than for AC,[22] which makes them attractive as electrode materials for high-rate supercapacitors,[18,22] conductive additive,[23] or substrate for hybrid electrodes employing redox-active materials such as metal oxides,[24] electroactive polymers,[25] or surface functional groups.[26]

With the limitation of double-layer capacitance to around 0.1 F/m^2 (normalized to electrode surface area), the energy storage capacity can be severely enhanced by use of redox-active materials.[6,27] The resulting devices benefit from fast and reversible redox reactions or intercalation processes between the ions and the surface of the electrode.[28] Depending on the charge-vs-voltage profile, redox-active media can be separated in capacitor-like systems (also known as pseudocapacitors; e.g., MnO_2, RuO_2, or MXene)[29−31] and battery-like systems (with clearly visible redox peaks; e.g., $Co(OH)_2$, polyaniline, or quinones).[25,32] Materials enabling Li^+ intercalation commonly belong to the latter group, for example, vanadium pentoxide (V_2O_5).[33−35] The distinction between capacitor- or battery-like behavior determines the choice of the most suitable performance metrics; while capacitors and intrinsic pseudocapacitive materials can be characterized by their specific capacitance (unit: F/g), the performance of battery-like devices should be described by means of specific capacity (unit: mAh/g) because of the nonconstant charge-vs-potential relation. For comparison between the two, the use of specific energy (Wh/kg) is preferred.[36,37]

The implementation of redox-active media to carbon electrodes faces many challenges. The direct use of most redox-active materials is not favorable given their poor electrical conductivity and low charge propagation.[2,38] Mixtures of conductive materials and redox-active materials, such as metal oxides, are often complicated by the need for small particle sizes and highly homogeneous phase distribution for optimized performance. The final goal is a hybrid electrode of highly conductive substrates decorated with thin layers or small particles of redox-active materials.[2,39] By this way, the high specific energy of battery-like devices may be matched with a rate handling performance known from capacitor-like systems. For that purpose, carbon nanotubes,[40−42] carbon onions,[24,43] and metal nanowires[44,45] have been investigated, among others, as substrate materials. The outer surface of these materials can be effectively decorated with redox-active materials by vapor deposition techniques like chemical vapor deposition and atomic layer deposition (ALD),[41,46,47] hydrothermal synthesis,[24,48] or drop-casting methods.[43]

ALD is a very versatile method to deposit nanoscale films of metal oxides on substrate surfaces. The process exhibits enhanced control over thickness and conformity of the fabricated coating due to its cyclic and self-limiting character.[49] Therefore, ALD has emerged as a promising tool to improve the performance of electrochemical devices, especially by decorating carbons with redox-active material, where a so-called nonline-of-sight deposition technique is required.[50] For example, Boukhalfa et al. coated carbon nanotubes with vanadium oxide via ALD and showed a linear increase in the tube diameter with increasing number of ALD cycles, thereby demonstrating the high conformity of the layer and high controllability of the thickness.[41] The amount of deposited vanadia strongly influenced the electrochemical performance of the hybrid electrode: for 100 ALD cycles, which corresponded to a layer thickness of about 10 nm, a specific capacitance of 530 F/g (177 mAh/g) in aqueous LiCl electrolyte was measured at a scan rate of 5 mV/s. Yet, for 500 ALD cycles, this value dropped by nearly 90% to about 60 F/g (20 mAh/g). The authors explained this behavior with the limited access of the electrolyte ions to the bulk of the coating and the drop in electrical conductivity with increasing metal oxide content.

Our work has been sparked by the pioneering work, among others, from the Yushin group[41] regarding the highly promising enhancement of electrochemical energy storage capacity by ALD decoration on carbon nanotubes as well as by the most recent work of Daubert et al.,[47] employing ALD on nanoporous carbons. Here, we present for the first time a comprehensive study on the impact of endohedral (AC) and exohedral (OLC) surface morphology on the ALD growth mechanism and the resulting electrochemical performance. Especially decorating directly free-standing polymer-bound electrodes is highly attractive because of beneficial electrical contacting between the carbon particles and the enhanced creation of an electrically conductive network. For contrast: metal oxide coated particles may increase the electrode resistance because of the high resistance of many redox active materials. Furthermore, vanadia nanocoatings are not fully stable in solvents used for electrode production, which is of no concern when already assembled electrodes are subject to the ALD process. The main issue with employing materials like activated carbon is related to clogging nanopores[47] in micrometer-sized particles, which may drastically reduce the energy storage capacity and even more severely limit the power performance. Also, it has not yet been established what the actual performance difference will be when comparing materials with high intraparticle porosity versus materials with just external surface area to survey competing effects of number of active sites versus ion transport.

2. EXPERIMENTAL SECTION

2.1. Preparation of Carbon Substrate Electrodes. OLCs were synthesized by thermal annealing of detonation nanodiamond with a diameter of 4−6 nm (NaBond Technologies), as described elsewhere.[20] The annealing process of the nanodiamond powder was carried out in a graphite crucible using a water cooled high temperature furnace with tungsten heater (Thermal Technology Inc.) in argon atmosphere at 1700 °C for 1 h (heating/cooling rate: 20 °C/min). Commercial YP-80F (Kuraray Chemicals Co.) was chosen as activated carbon (AC).

To fabricate free-standing carbon electrodes, carbon powder was mixed with 5 wt % (AC) or 10 wt % (carbon onions) of polytetrafluoroethylene binder (PTFE, 60 wt % solution in water, Sigma-Aldrich) and ethanol. The obtained slurry was then rolled to a 50−60 μm thick electrode. Electrodes were dried in a vacuum oven (2×10^3 Pa) for about 6 h at 120 °C prior to further use. Further information on the electrode fabrication procedure is found in ref 51.

2.2. ALD of Redox-Active Material on Carbon Substrate Electrodes. The coating process was performed with an open-load ALD system (OpAL; Oxford Instruments). The reactor is surrounded by a custom-made inert gas glovebox (M. Braun Inertgas-Systeme) to ensure dry loading of the samples. Vanadium oxide layers were synthesized from vanadium(V)-oxytriisopropoxide (VOTIP; SAFC Hitech) as metalorganic precursor and deionized water vapor (Milli-Q, Merck) as reactant gas. The VOTIP pot was heated to 45 °C, and the gases entered the ALD reactor during successive 20 s dosage steps. After each dosage step, argon was used to purge the reactor for 10 s. At the end of each cycle, the reactor was evacuated for 8 s. The table temperature inside the reactor was kept at 180 °C. The PTFE-bound carbon electrodes were mounted vertically on the heated table so that

DOI: 10.1021/acs.chemmater.6b00738
Chem. Mater. 2016, 28, 2802−2813

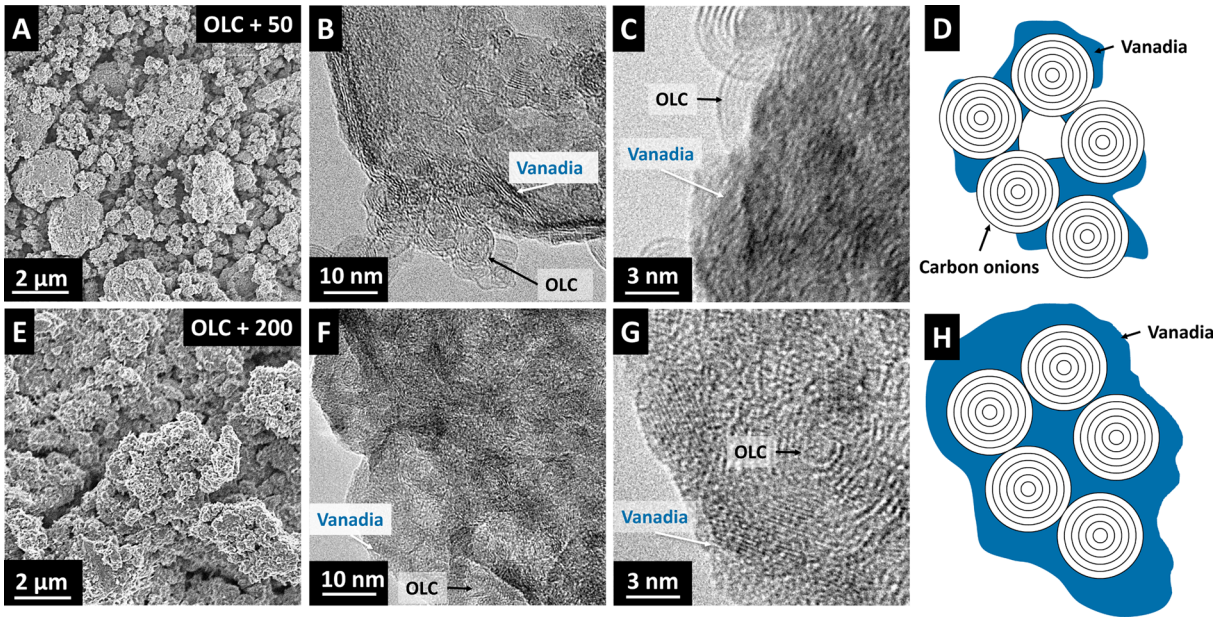

Figure 1. Scanning and transmission electron micrographs of carbon onion hybrid electrodes coated with (A, B, C) 50 ALD cycles and (E, F, G) 200 ALD-cycles as well as (D, H) schematic illustrations of the respective coating structures.

the precursor and reactant gas were able to penetrate the electrodes from both sides. Before the deposition process, the electrodes were treated with oxygen plasma for 5 min to enrich their surfaces in functional groups. By that way, the homogeneity of VOTIP adsorption on the carbon substrate in the first ALD cycle was enhanced. The resulting vanadium oxide coated electrodes are further referred to as carbon/vanadia hybrids. The nomenclature of samples (e.g., OLC +100) means the carbon substrate coated with 100 ALD cycles of vanadia.

In preliminary tests, instead of coating PTFE-bound electrodes, we also surveyed to coat carbon particles instead. However, the metal oxide coatings were not stable when exposed to the ethanol-based electrode preparation. Use of PTFE-bound electrodes was also more beneficial since carbon−carbon contacts were not negatively affected by the coating process and improved scalability was ensured.

2.3. Structural Characterization. Scanning electron microscopy (SEM) was carried out employing a JSM-7500F (JEOL) operating at 3 kV. Electrodes were cut with a razor blade and attached to a steel sample holder by carbon tape to take cross-sectional images. Energy dispersive X-ray (EDX) spectra were recorded at 15 kV with an X-Max-150 (Oxford Instruments) attached to the SEM. Transmission electron microscopy (TEM) was performed with a 2100F system (JEOL) at 200 kV. The samples were prepared by dispersing and sonicating the electrodes in isopropanol and placed on a copper grid with a lacey carbon film (Gatan Inc.).

For X-ray diffraction (XRD) experiments, a D8 Advance XRD (Bruker AXS) diffractometer with a copper X-ray source ($Cu_{K\alpha}$, 40 kV, 40 mA) and a nickel filter was used. All measurements were performed in a range from 10−60° 2θ with a step width of 0.02° 2θ.

Raman spectra were recorded by a Renishaw inVia Raman Microscope employing an Nd:YAG laser with an excitation wavelength of 532 nm. A grating with 2400 lines/mm and a 50× objective were used to reach a spectral resolution of about 1.2 cm^{-1}. The laser spot on the sample was about 1 μm in diameter at a power of 2.5 mW. The acquisition time of each spectrum was 30 s, and 10 accumulations were applied.

Nitrogen gas sorption analysis (GSA) was performed with an Autosorb iQ System (Quantachrome). The PTFE-bound electrodes and the carbon/vanadia hybrid electrodes were degassed at 150 °C for 10 h under vacuum (100 Pa) to remove adsorbed water and gas molecules. For the GSA, the variation of relative pressure of liquid nitrogen (−196 °C) from 5 × 10^{-7} to 1.0 occurred in 68 steps. The SSA was calculated with the Brunauer−Emmett−Teller (BET) equation[52] in the linear range of the relative pressure between 0.01 and 0.20 using the ASQwin-software. The pore size distribution (PSD), as well as the total pore volume, was calculated by quenched-solid density functional theory (QSDFT).[53] A model for slit-shaped pores between 0.56 and 37.5 nm was employed.

Energy filtered imaging (EFTEM) was conducted on Libra 120 transmission electron microscope (Carl Zeiss AG) operated at 120 keV. The specimen was prepared by dispersing vanadium oxide coated carbon onion powder in tetrahydrofuran (THF) followed by placing a drop on a lacey carbon film TEM grid. The TEM grid was dried at 50 °C to remove traces of THF before inserting into the TEM instrument.

2.4. Electrochemical Characterization. The electrochemical performance was characterized using a three-electrode setup (half-cell) outlined in more detail in ref 54. The carbon/vanadia hybrids with different vanadia-loadings were employed as working electrodes. The mass of the working electrodes was between 1 and 2 mg. The oversized counter electrode was PTFE-bound AC (YP-80F, Kuraray) with a mass of about 15 mg. As reference electrode, PTFE-bound activated carbon (YP-50F, Kuraray) was chosen.[55] The current collectors consisted of carbon-coated, 12 mm diameter aluminum foil (Zflo 2653, Exopack Technologies) and 13 mm glass fiber mat as separator (GF/D, Whatman). After assembly, the cells were dried at 120 °C in a vacuum oven overnight to remove any moisture. The cells were then electrolyte filled in an inert gas glovebox (MBraun Labmaster 130, O_2 and H_2O < 1 ppm) with 1 M $LiClO_4$ (battery grade, Sigma-Aldrich) in acetonitrile (battery grade, BASF). A two-electrode setup (full-cell) was employed to further characterize hybrid electrodes with 100 ALD cycles. Therefore, both a charge balanced, asymmetric setup with carbon/vanadia and activated carbon (YP-80F, Kuraray) and a symmetric setup with two carbon/vanadia electrodes of the same mass were utilized. In the charge balanced setup, the mass of the activated carbon electrode was chosen as three-fold the mass of carbon/vanadia electrodes. All other assembly steps were chosen equivalently to the three-electrode setup described above.

The electrochemical measurements were carried out with a potentiostat/galvanostat (VSP300, Bio-Logic) and included cyclic voltammetry (CV) and galvanostatic charge/discharge with potential limitation (GCPL). Cyclic voltammograms were recorded in a potential window from −1.2 V to +1.2 V versus YP-50F reference for half-cells and 0 V to +2.5 V for full-cells, respectively, with scanning rates of 1 mV/s and 10 mV/s. For half-cells, galvanostatic charge/discharge cycling was carried out by between 0 and −1.2 V, for full-

DOI: 10.1021/acs.chemmater.6b00738
Chem. Mater. 2016, 28, 2802−2813

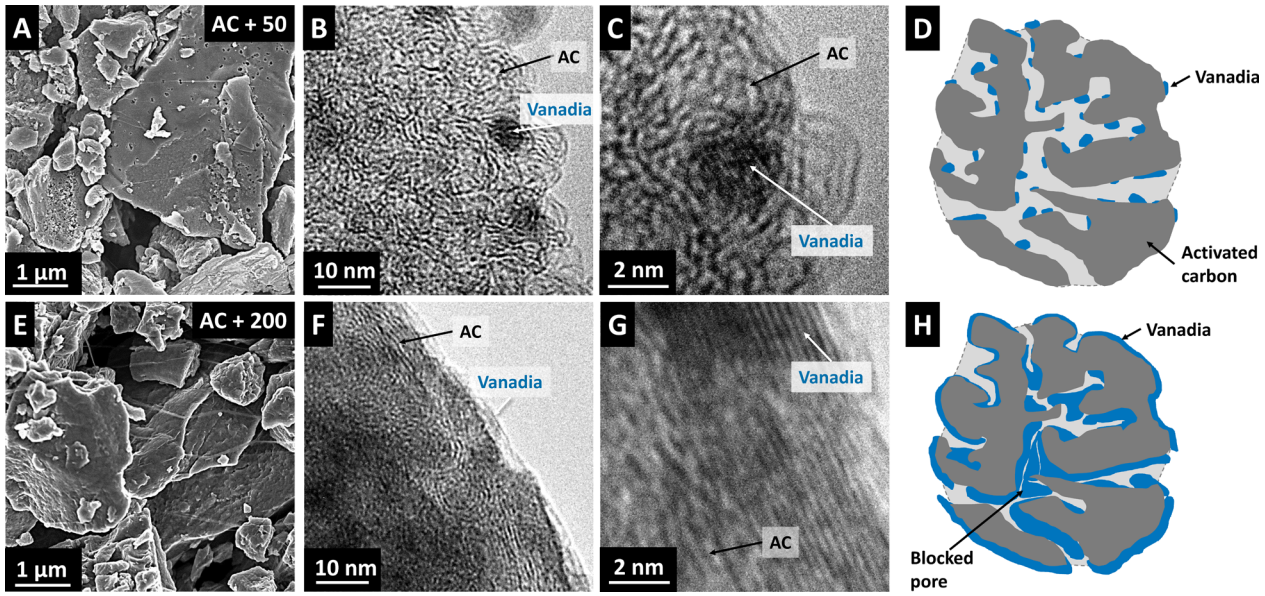

Figure 2. Scanning and transmission electron micrographs of activated carbon hybrid electrodes coated with (A, B, C) 50 ALD cycles and (E, F, G) 200 ALD-cycles as well as (D, H) schematic illustrations of the respective coating structures.

cells between 0 and +2.5 V. The applied specific currents ranged from 0.05−10 A/g, with respect to the active mass of the working electrode in half-cells, or to the active mass of both electrodes in full-cells, respectively (excluding the mass of the PTFE-binder, which differs for AC and carbon onion electrodes). The specific (gravimetric) capacity C_{sp} was calculated from the GCPL data by integration of the discharge current over the discharge time according to eq 1:

$$C_{sp} = \frac{\int_{t_0}^{t} I \, dt}{m} \tag{1}$$

where I is the current, t the discharge time, and m the total mass of the working electrode (half-cells) or the total mass of both electrodes (full-cells), respectively.

The specific energy E_{sp} of full-cells was calculated by integration of the voltage over the discharge time by employing eq 2:

$$E_{sp} = \frac{I \int_{t(U_{max})}^{t(U_{min})} U(t) \, dt}{m} \tag{2}$$

where $U(t)$ is the time-dependent voltage and m the total mass of both electrodes. Long-term stability tests were performed in half-cells by charge/discharge from −1.2 to 0 V with a specific current of 1.0 A/g.

3. RESULTS AND DISCUSSION

3.1. Structural Characterization. Carbon onions were derived from detonation nanodiamond (ND) powder by thermal annealing at 1700 °C (see Supporting Information, Figure S1), which caused transformation of the diamond core and amorphous layers of ND to graphitic carbon shells, resulting in carbon onion particles. These particles form agglomerates of up to 2 μm, which are built up by primary aggregates ranging from 10−100 nm in size (see Supporting Information, Figure S2), as has been demonstrated before.[23] The agglomeration of carbon onions during the synthesis is resulting from agglomeration of the precursor, high temperature treatment induced particle−particle sintering, and carbon redistribution processes.[56] Carbon onion electrodes have been coated with different mass loadings of vanadium oxide, and their surface morphology has been studied via SEM and TEM and is shown in Figure 1. From a macroscopic point of view, no major structural changes were detected after the ALD process using SEM (Figure 1A,E). As seen from the TEM images in Figure 1, panels B and C and as schematically exemplified in Figure 1, panel D, a partial coverage of carbon onion surfaces with vanadia layers was obtained at a low mass loading after 50 ALD cycles. Sample OLC + 200 (Figure 1F−H) shows a dense particle coating, which exhibits a mixture of crystalline and amorphous vanadia structures. The interparticle space is fully covered by the vanadia coating; hence, there is no observable pore space inside the carbon onion agglomerates. The TEM micrographs show that the growth of vanadia layers on carbon onion particles does not occur in a completely continuous manner on a nanoscopic level. After 50 ALD cycles, the carbon onion particles were only partially coated. This can be explained by the lack of initial adsorption sites for the VOTIP precursor molecules.[57] As a consequence, small domains of vanadia nucleate distributed over the carbon onion surfaces and start growing. After 200 ALD cycles, these vanadia domains merged, and the surface is more continuously coated. Crystalline vanadia is preferentially found on the outside of agglomerates, while interparticle space inside the agglomerates mostly consists of amorphous vanadia in absence of required space for crystal growth. The distribution of vanadia within the primary particles was evaluated using EFTEM and was found to be relatively homogeneous (Supporting Information, Figure S3). It is demonstrated that vanadia growth occurred mostly inside the agglomerates, filling interparticle space, rather than forming thick layers on the outer surface of carbon onion primary particles.

AC consists of porous and incompletely graphitic carbon particles (Figure 2) with a size distribution between 1 and 5 μm, which is in accordance with data from sedimentation analysis (Supporting Information, Figure S2). The shape of the particles is not uniform and more polygonal compared to the highly spherical and isometric carbon onions. Large macropores of different sizes are readily seen on the surfaces of the particles with electron microscopy (Figure 2A,E). AC exhibits few interparticle contacts, and connections are mainly formed by PTFE-fibers in the electrode. Inside the AC particles that were

DOI: 10.1021/acs.chemmater.6b00738
Chem. Mater. 2016, 28, 2802−2813

coated with 50 ALD cycles, several vanadia domains with a diameter of about 1 nm were detected by TEM (Figure 2B,C), while no vanadia is present outside of these spots. Also, on the outer surface of AC particles, only little coating is visible, indicating a preferential initial adsorption of VOTIP precursor inside the nanopores. These domains inside the AC particles grow with an increasing number of ALD cycles. At higher mass loadings, a rather homogeneous distribution of vanadia in the intraparticle space (Figure 2F,G) is observed. The dense filling is a result of the merging of growing domains.

To examine the coating arrangement fabricated via ALD in the cross-section of the about 50 μm thick, free-standing electrodes, energy dispersive X-ray spectroscopy (EDX) was carried out. As indicated by the homogeneous intensity of oxygen and vanadium element mappings (Supporting Information, Figure S4), a highly uniform distribution of vanadia through the entire electrode thickness was achieved by choosing suitable ALD parameters.

The vanadia loading in the hybrid electrodes was determined by weighing the electrodes prior to and after the ALD process. The relation between the number of ALD cycles and the relative mass gain is illustrated in Figure 3. It is demonstrated

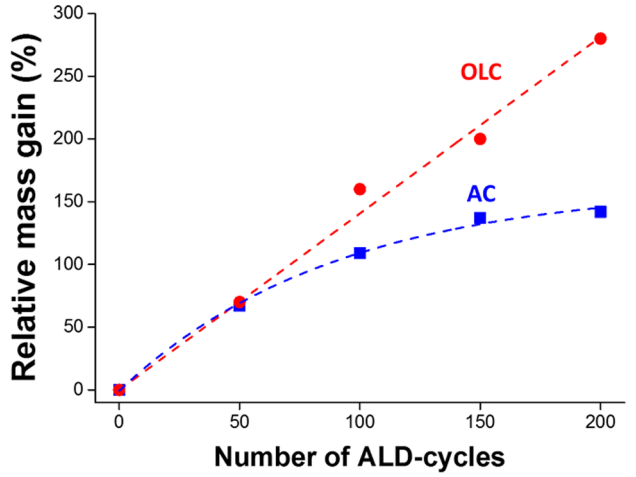

Figure 3. Relative mass gain of OLC and AC hybrid electrodes after the ALD process, with respect to the initial mass.

that the vanadia loading increases linearly with the number of ALD cycles for carbon onion electrodes, with an average mass gain of about 1.4% per cycle, with respect to the initial mass. This linearity demonstrates the highly conformal ALD deposition enabled by choosing a suitable dosage time of 20 s for sufficient diffusion of VOTIP precursor and reaction gas molecules to all available adsorption sites in the OLC electrode and for complete reaction during each ALD cycle. The mass gain for AC converges to a saturation for higher numbers of ALD cycles. The nonlinear mass gain behavior is a consequence of the high inner porosity of AC. With increasing vanadia loading, blocking of subnanometer pores in the micrometer-sized particles reduces the accessible surface area for VOTIP molecules on which to adsorb. Consequently, the mass increase for one ALD cycle decreases from a 1.3% after 50 cycles to 0.7% after 200 cycles.

X-ray diffractograms of the hybrid electrodes (Supporting Information, Figure S5) exhibited very low peak intensities for vanadia, which make the data insufficient for a detailed description of the crystal structure. It can rather be regarded as an indication for a predominately amorphous/nanocrystalline vanadia of vanadia. To provide a more detailed structural characterization of the coating material, Raman spectroscopy was carried out.

The Raman spectrum of carbon onion hybrid electrodes contains several characteristic vanadia peaks (Figure 4A). The peak corresponding to the relative motions of two V_2O_5 unit cells is located at 142 cm^{-1}[58−60] and can be found for sample OLC+50, but for the other three mass loadings of vanadia, the corresponding peak is shifted to 158 cm^{-1}. Similarly, the peak attributed to the V═O stretching mode, found in V_2O_5, V_2O_3, and VO_2, is reported at 992 cm^{-1} in literature,[58−60] which is in accordance to the peak observed for OLC+50. For the other three samples, the peak is shifted to a value of 1024 cm^{-1}. The two peaks at 267 and 406 cm^{-1}, also characteristic for the V═O bond,[58−60] are found in all recorded spectra, with the latter only exhibiting a sharp shape for the OLC+50 sample. The peak occurring at 516 cm^{-1} represents a triply coordinated oxygen bond (present in V_2O_5), and the peak at 704 cm^{-1} a doubly coordinated oxygen bond (present in VO_2 and V_2O_3).[58−60] The results suggest the presence of vanadia in three oxidation states (III−V), with the fully oxidized and V_2O_5 being the predominant phase, indicated by the peaks with most intensity at 142, 158, and 516 cm^{-1}. The spectrum of OLC + 50 is in best accordance with the literature values. For higher vanadia loadings, the peak shifting suggests distortions of the V═O bond, as have been described in literature for V_2O_5.[58,61]

The Raman spectrum of AC hybrid electrodes only exhibits a very low intensity of the characteristic V_2O_5 peak at 142 or 158 cm^{-1} (Figure 4B) as a consequence of the growth of mostly amorphous vanadia in the intraparticle space. The exclusively external surface area of carbon onions provides favorable conditions for crystalline growth of vanadia layers, contrary to the microporous internal surface area of AC particles. Consequently, OLC/vanadia electrodes contain proportionally more crystalline vanadia, therefore showing higher Raman signal intensities.

An analysis of the D- and G-peaks is conducted with baseline-subtracted and D-peak normalized spectra, given in Figure 4, panels C and D. For both carbon materials after coating, a shift of D- and G-peak position to higher vibration frequencies is clearly visible compared to the uncoated carbon materials. Furthermore, the full width at half-maximum (FWHM) of the D-peaks increases by about 20% for all coated electrodes, while the FWHM of G-peaks remains roughly constant (Figure 4E). A decreasing areal intensity ratio of the D- and G-peak (I_D/I_G) is detected for coated carbon onion electrodes, while I_D/I_G increases with higher ALD cycle numbers for coated activated carbon (Figure 4F). The changes in peak position, FWHM, and areal intensity ratio appear to be irrespective of the vanadia loading, as the spectra of all coated electrodes are virtually identical. Thus, we can see that some initial change of the carbon structure of AC and OLC takes place after a few ALD cycles without significant further changes. The reason for this behavior is the formation of the vanadia/carbon interface during the beginning of the coating process. With a higher number of ALD cycles, the layer growth is mostly realized by vanadia/vanadia reactions, which have no impact on the carbon structure. The peak shifting has been described for the G-peak of disordered graphite in literature.[62,63] While the effect is not observable for pure graphite, the introduction of disorder is linked with a proportionally growing G-peak shifting.[62] We suspect the observed carbon disordering of

DOI: 10.1021/acs.chemmater.6b00738
Chem. Mater. 2016, 28, 2802−2813

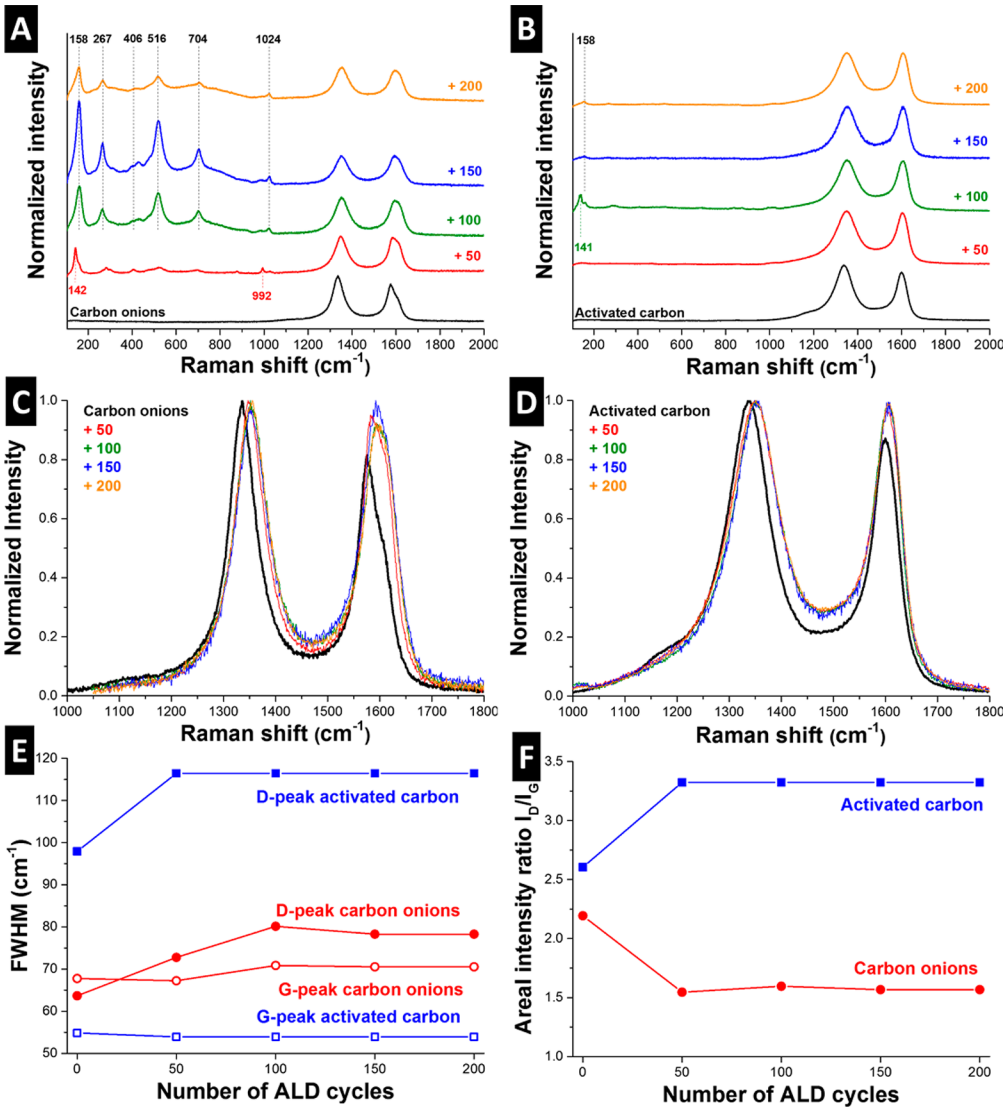

Figure 4. Raman spectra (overview) of (A) carbon onion and (B) activated carbon hybrid electrodes, characteristic vanadia peaks are labeled accordingly. Detailed spectra of D- and G-peaks for (C) carbon onion and (D) activated carbon hybrid electrodes as well as (E) the full width at half-maximum (FWHM) and (F) the areal intensity ratio as a function of coating thickness highlight the changes in carbon structure introduced by vanadia coatings.

coated electrodes to be the consequence of surface stresses induced by a nonepitaxial growth of vanadia layers. Thereby, we introduce external stresses to the hexagonal arrays of sp^2-carbon that cause a change in vibrational modes of in-plane bond-stretching motions.[63] This analysis is in conclusion with the increasing FWHM of the D-peak for both carbons, which is indicative for a reduction in long-range ordering of graphitic carbon.[20]

An increasing I_D/I_G ratio is generally associated with structural disorder and the introduction of defects in carbon.[64] The increasing I_D/I_G ratio for coated activated carbons supports the former observations, whereas the decreasing I_D/I_G ratio for carbon onions can be explained by the model of Ferrari and Robertson.[63] For crystalline domain sizes below a diameter of about 2 nm, I_D is considered to be proportional to the probability of finding sp^2-hybridized carbon rings,[63] and consequently, a decreasing I_D/I_G ratio suggests a higher degree of disorder. In the case of carbon onions, the domain size of hexagonal sp^2-carbon rings is further reduced under the influence of external stresses. Thus, a drop to or below 2 nm of the remaining crystalline clusters can be assumed, and therefore, the drop in I_D/I_G is in agreement with the findings for peak shifting and FWHM.

The impact of the ALD coating on porosity and pore size distribution of the carbon electrodes is evaluated by nitrogen gas sorption analysis. The isotherms of carbon onion hybrid electrodes, as shown in Figure 5, panel A, exhibit a typical type II shape with H3 hysteresis of the most recent 2015 IUPAC classification,[65] which is evident for a nonporous nanoparticle structure. With increasing vanadia loading, the specific volume of adsorbed nitrogen decreases due to the density increase of the hybrid electrode and partial filling of interparticle space. The isotherm shape of AC-based hybrid electrodes up to 100 ALD cycles correspond to type I(b), as seen from Figure 5, panel B. These electrodes exhibit a steep increase in adsorbed nitrogen at low pressures, which is associated with the filling of micropores. The hysteresis loops are smaller than for carbon onion electrodes and match with type H4, which is correlated with a micro- and mesoporous carbon structure. Only a very small amount of nitrogen was adsorbed on samples AC+150

DOI: 10.1021/acs.chemmater.6b00738
Chem. Mater. 2016, 28, 2802−2813

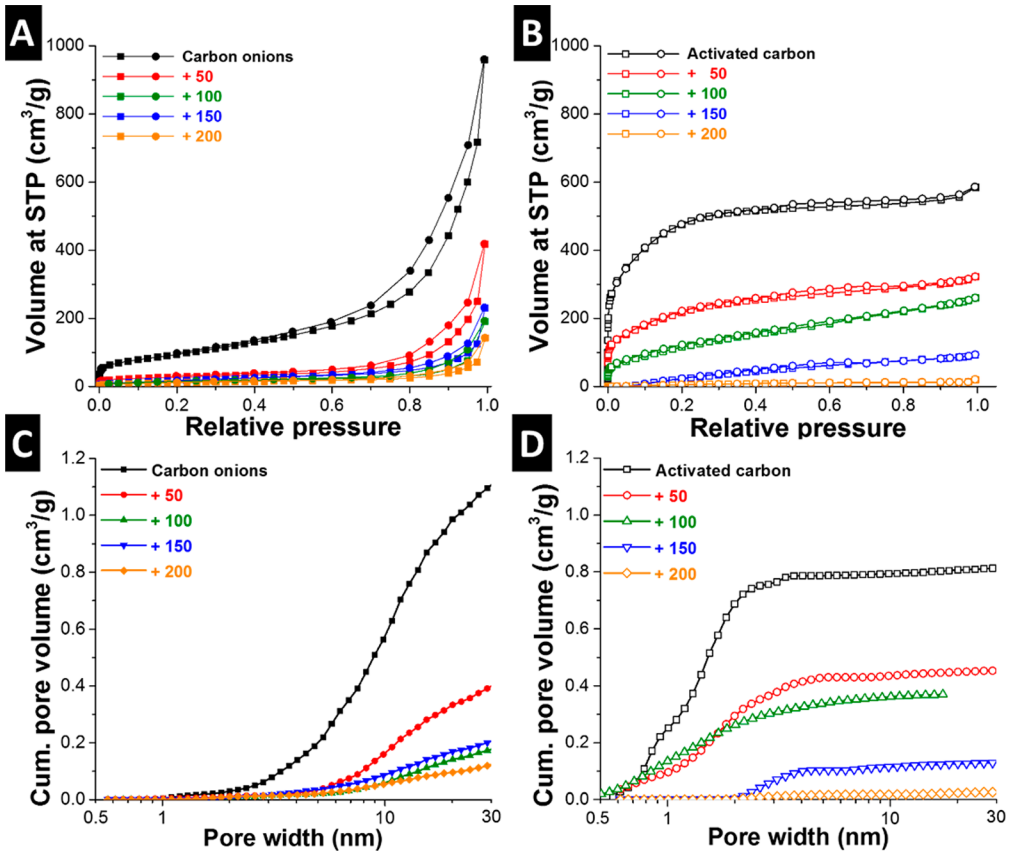

Figure 5. Nitrogen sorption isotherms at standard temperature and pressure (STP) and specific cumulative pore volume of (A, C) carbon onion and (B, D) activated carbon hybrid electrodes.

and AC+200. Their isotherm shape is best described as type-III-like, corresponding to nonporous or macroporous materials with weak adsorbent–adsorbate interactions.[65] The reason for this is the extensive micro- and mesopore blocking for higher amounts of vanadia coating. These observations are corroborated by the calculated SSAs (BET), which are listed in Table 1.

Table 1. Comparison of SSA_{BET}, SSA_{DFT}, and Pore Volume of Carbon Onion and Activated Carbon Hybrid Electrodes

material	SSA_{BET} (m^2/g)	SSA_{DFT} (m^2/g)	pore volume (cm^3/g)
carbon onions	352	311	0.93
+ 50	98	98	0.31
+ 100	50	44	0.12
+ 150	69	53	0.15
+ 200	42	33	0.09
activated carbon	1759	1289	0.86
+ 50	800	643	0.48
+ 100	458	323	0.38
+ 150	237	77	0.13
+ 200	28	13	0.02

With increasing vanadia loading, SSA_{BET} and pore volume decreased for both types of hybrid electrodes. This decrease is mainly caused by two factors. First, the skeletal and geometric density of the hybrid electrode increases with a growing amount of comparably high density vanadia (V_2O_5, 3.36 g/cm^3; VO_2, 4.34 g/cm^3) that is primarily occupying internal pore volume and interparticle voids. The second factor is attributed to pore blocking by the vanadia coating, which makes surface area inside micropores inaccessible, as it is mainly observed for AC hybrid electrodes.

The pore size distribution (PSD) of carbon onion electrodes is characterized by micropores around 1 nm, formed by direct particle contacts, and a high amount of mesopores, formed by intercluster voids between the nanoscopic primary particles (Figure 5C).[20] Uncoated OLCs are dominated by mesopores starting at about 2 nm, while pores of coated samples are mostly above 6 nm in size. The general shape of all OLC pore size distribution curves is similar, only shifted toward larger pore widths and smaller total volume with increasing number of ALD cycles. Therefore, it can be assumed that mostly small mesopores between the primary particles in the range of about 2–6 nm were filled by vanadia during the ALD process. The pore structure of AC electrodes (Figure 5D) for samples AC+50 and AC+100 shares many similarities with uncoated AC. The amount of micropores up to 0.8 nm is roughly equal (ca. 0.1 cm^3/g), and a decrease in pore volume is found for pores starting at a width of about 1 nm up to 100 ALD cycles. These findings show that vanadia growth preferentially occurs in pores above 1 nm since there is insufficient space for initial VOTIP adsorption inside subnanometer micropores, as confirmed in a previous study.[47] Complete blocking of these micropores is observed in advanced growth stages of vanadia, for samples AC+150 and AC+200, which is caused by layers covering the micropore necks.

3.2. Electrochemical Characterization. CV for carbon onion electrodes was carried out in half-cells (i.e., three electrode setup) to first characterize the performance of hybrid electrodes with respect to the coating thickness. The CVs of

DOI: 10.1021/acs.chemmater.6b00738
Chem. Mater. 2016, 28, 2802–2813

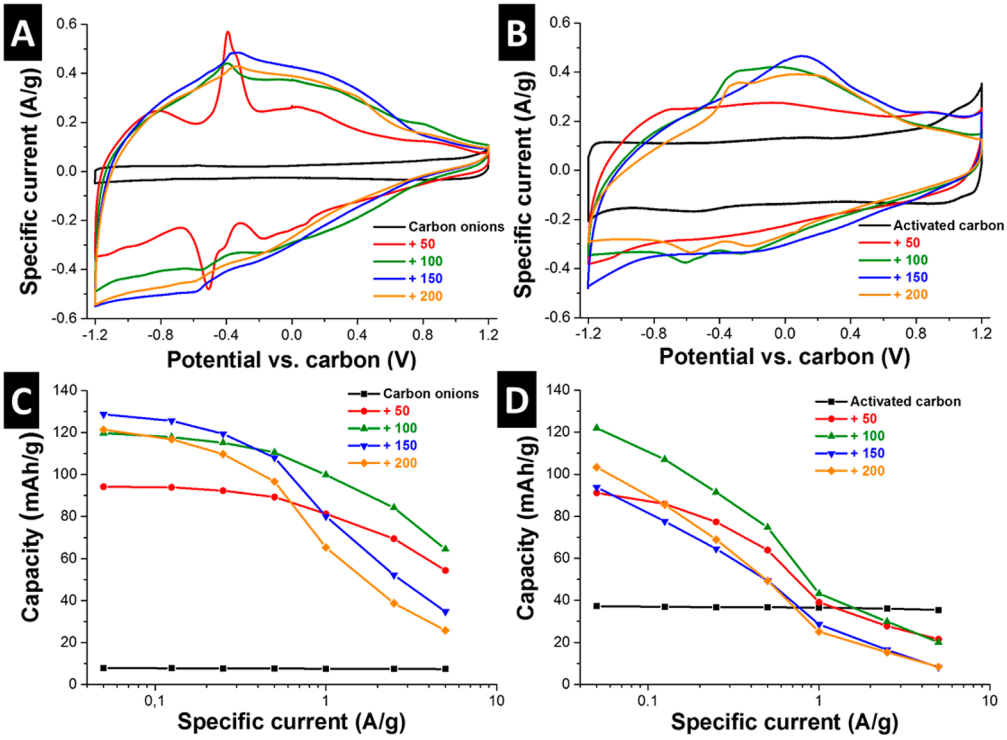

Figure 6. Cyclic voltammograms measured at 1 mV/s and specific capacity values derived from integrating galvanostatic discharge curves for (A, C) carbon onion and (B, D) activated carbon hybrid electrodes.

uncoated carbon onion electrodes exhibit a rectangular shape (Figure 6A), which is indicative of a nearly ideal capacitive behavior.[36,66] The symmetric, slight current increase observed at higher voltages is not related to noncapacitive reactions but is rather caused by an increase in the density of states of charge carries for highly graphitized carbon electrodes at high potentials ("butterfly-effect") and has been discussed elsewhere in more detail.[54,67] The specific current of OLC/vanadia hybrid electrodes at 1 mV/s significantly increased compared to uncoated carbon onions, particularly for negative potentials (Figure 6A). The current increase can be distinguished as either an amplification of the rectangular signal, which is typical for pseudocapacitors, or as formation of two peaks, characteristic for battery-like devices.[28] These findings are similar to other carbon/vanadia systems that have been investigated before such as CNT/vanadia[41] or nanoporous carbon/vanadia.[47] It can be assumed that Faradaic reactions at the electrode/electrolyte interface and intercalation reactions of lithium-ions in the coating both contribute to the current increase. For sample OLC+50, two redox peaks are clearly visible at −0.4 V versus carbon for charging and −0.5 V versus carbon for discharging, indicating a potential-dependent reaction, which is in alignment with peak positions for lithium intercalation.[68,69] With an increasing number of ALD cycles, the peaks are less pronounced and the current increase associated with the potential dependent reaction is stretched over a larger potential range.[38] The change of the CV shape for different coating thicknesses gives information about the kinetics of the reactions. The pronounced peaks for OLC+50 are the result of a high reaction rate of lithium intercalation in V_2O_5, whereas the peak stretching for higher numbers of ALD cycles is caused by slower reaction kinetics. The main reason is the growing coating thickness that results in a decrease in electrical conductivity due to the less conductive vanadia[42,70] and longer diffusion paths for lithium ions to the reaction sites,[71] both inhibiting high reaction rates. Also, as discussed in the Raman data section, OLC+50 exhibited the highest degree of structural V_2O_5 ordering, which contributes to enhanced intercalation kinetics.

The CVs of AC/vanadia hybrid electrodes (Figure 6B) reveal a higher charge storage capacity compared to uncoated AC. The shape of the CV curves reveals similarities with OLC/vanadia, except for the sample AC+50. Here, in contrast to OLC+50, no typical battery-like redox peaks can be observed, and a mostly (pseudo)capacitive behavior is exhibited. Vanadia growth on AC surfaces is initiated by the formation of few nanodomains, mostly inside the porous AC particles, which are about 1 nm in size after 50 ALD cycles (Figure 2B,C). From the Raman data, it was concluded that these domains do not exhibit a crystalline structure (Figure 4B), and therefore, no high intercalation capacity for lithium ions is expected. Thus, the increase in specific capacity for AC+50 is mainly attributed to Faradaic (surface) reactions. The emergence of highly broad and ill-contoured redox peaks at a higher number of ALD cycles is resulting from the converging vanadia nuclei, which begin to form crystalline structures that mostly consist of V_2O_5 and promote lithium intercalation.[34]

Galvanostatic charge/discharge measurements were carried out by applying a negative potential to the working electrode versus carbon in anticipation of redox reactions of Li^+ with the vanadia layers of the hybrid electrodes (Figure 6C,D). It can be seen that the discharge capacity of the OLC/vanadia electrodes was about one order of magnitude above uncoated carbon onion electrodes at low specific currents (Figure 6C). With increasing specific current, the specific capacity of the hybrid electrodes decreased, while carbon onion electrodes performed on a relatively constant level. It can be observed that higher coating thickness results in less capacity retention at high

DOI: 10.1021/acs.chemmater.6b00738
Chem. Mater. 2016, 28, 2802−2813

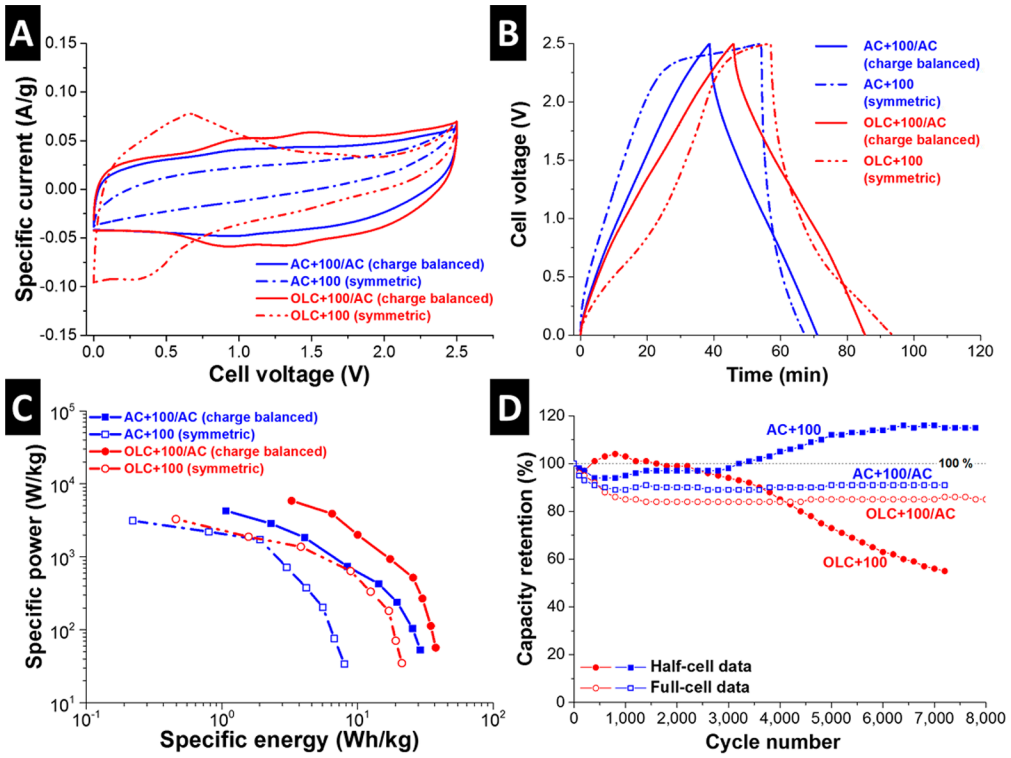

Figure 7. (A) Cyclic voltammograms measured at 1 mV/s, (B) galvanostatic charge−discharge profiles measured at 0.05 A/g, and (C) Ragone plot for charge balanced (against activated carbon, YP-80F) and symmetrical full-cells of OLC+100 and AC+100 hybrid electrodes. (D) Cycling stability test of AC+100 and OLC+100 in half cells, and AC+100/AC and OLC+100/AC in charge balanced full-cells at a specific current of 1 A/g.

specific currents. The performance decline for thicker coatings is a result of longer diffusion paths and the insulating effect of vanadia, which leads to charge limitations particularly at high sweeping rates. At a low specific current of 0.05 A/g, OLC+150 exhibited with 129 mAh/g the highest capacity of all studied hybrid electrodes (to provide a better comparability: when (incorrectly) expressed as capacitance, this value would correspond to 387 F/g). The value dropped with an increasing specific current, and a capacity retention of about 27% was observed at 5 A/g. In comparison, OLC+100 showed a comparably high capacity of 120 mAh/g at 0.05 A/g while still retaining 53% of its initial capacity at 5 A/g. The rate handling performance of OLC+50 and OLC+100 is similar and comparable to uncoated carbon onions below a current density of 1 A/g. The capacity of the electrode with 150 ALD cycles is only marginally superior to 100 ALD cycles at a very low specific current. This suggests that most reactions take place at the coating surface, while only little lithium intercalation into the "bulk" of the coating takes place as supported by the lower initial capacity of OLC+200. This electrochemically inactive vanadia can be considered as dead mass, decreasing the specific performance values of the electrode. A reason for this behavior is that the vanadia coatings exhibit only partial crystallinity, while substantial amounts of the coating show a distorted or amorphous structure, which is not favorable for lithium intercalation.[34] Overall, the hybrid electrode with 100 ALD cycles showed the most attractive electrochemical properties, with a good compromise between high initial capacity and good rate handling performance.

The discharge capacity of AC/vanadia hybrid electrodes at a low current density was about 2−3-times higher than that of uncoated AC. With higher current densities, the capacity values dropped increasingly with a higher coating thickness, exhibiting retentions between 24% (for 50 ALD-cycles) and 8% (for 200 ALD-cycles) at 5 A/g. At a low current density of 0.05 A/g, AC +100 showed the highest capacity of all AC/vanadia electrodes with 122 mAh/g, which is comparable to OLC+100. Yet, with increasing current densities, the observed drop in capacity was more severe as for carbon onion electrodes. Above specific currents of 1 A/g, all AC/vanadia electrodes showed less capacity than uncoated AC. Besides the aforementioned insulating effect of vanadia, the inferior electrical conductivity of AC, which is about one order of magnitude lower than for carbon onions,[23] is another reason for the more severe decline in performance at higher scanning rates. Furthermore, this behavior can be related to the microporous structure of AC. The vanadia coating is responsible for micropore blocking inside the AC particles and causing a large reduction in accessible SSA,[47] as observed by GSA (Figure 5B). Also, diffusion paths in the porous network of AC become narrower, thus increasing the diffusion resistance for ions. Obviously, a high electrical conductivity of the carbon substrate material is a requirement for good rate handling characteristics of hybrid electrodes. Vanadia coatings introduced to AC electrodes are only desirable for low rate applications, and a coating thickness, equivalent to 100 ALD cycles in this work, should not be exceeded to avoid extensive pore blocking and insulating phenomena.

It was demonstrated that both hybrid electrodes exhibited the best performance when loaded with 100 ALD cycles of vanadia. Therefore, the electrochemical performance of these hybrid electrodes is further investigated both in charge balanced full-cells against activated carbon and in symmetrical full-cells. The CV (Figure 7A) of charge balanced OLC+100/AC exhibits a slightly higher specific current than AC+100/AC as a result of small redox peaks at cell voltages of around +1.0 V and +1.3 V

DOI: 10.1021/acs.chemmater.6b00738
Chem. Mater. 2016, 28, 2802−2813

cell voltage. At a cell voltage of +1.0 V, the applied potential at the OLC+100 electrode in the charge balanced system is at about −0.5 V, which is in alignment with the redox peaks observed in half-cells. In comparison, the specific current of symmetrical full-cells is extensively reduced, especially at higher cell voltages. This behavior is explained by charge limitations caused at the positive electrode, which are a consequence of the inferior performance of the hybrid electrodes in the positive potential area, as has been demonstrated by the CVs of half-cells (Figure 6A,B).

Galvanostatic charge−discharge profiles (Figure 7B) were used to calculate the specific energy and specific power as used for a Ragone plot (Figure 7C). The performance of charge balanced full-cells is superior compared to symmetrical full-cells in both specific energy and specific power. OLC+100/AC exhibits specific energies of 38 Wh/kg and 3.3 Wh/kg at specific powers of 57 W/kg and 5.9 kW/kg, respectively. In comparison, AC+100/AC shows a performance of 29 Wh/kg (1.1 Wh/kg) at 53 W/kg (4.3 kW/kg). The low performance of symmetrical cells is effected by the rapid voltage drop in the discharge cycle (Figure 7B). This low cycle efficiency is explained by the disparate electrochemical behavior of the carbon/vanadia hybrid electrodes in the positive and negative potential window. Therefore, the two electrodes are disproportionally charged, and the resulting potential at the positive electrode exceeds the stability window of the electrolyte. Superior performance can only be found for asymmetrical cells, where the carbon/vanadia hybrid material is used as a negative electrode.

Stability testing was carried out in both a half-cell setup with AC+100 and OLC+100 hybrid electrodes, and in charge balanced full-cells (AC+100/AC and OLC+100/AC) via galvanostatic charge−discharge at 1 A/g (Figure 7D). Both half-cells retained about 95% of their initial discharge capacity up to 3000 cycles. Afterward, OLC+100 exhibited a steady capacity fading of about 1% every 100 cycles, while the capacity of AC+100 increased to about 115% of the initial value after 8000 cycles. Long-term cycling leads to electrochemical degradation of vanadia, which causes a reduced redox activity and therefore a decrease in performance of the OLC+100 hybrid electrodes. For the AC+100 hybrid electrodes, though, the electrochemical degradation of vanadia gave rise to a partial clearance of blocked channels inside the microporous AC particles, which benefited the ion mobility and thereby decreased the electrodes resistivity, as seen from the reduction of the IR drop (Supporting Information, Figure S6). The result is a slight increase in capacity after 3000 cycles. The charge balanced full-cells exhibited a minor drop in discharge capacity after a few hundred cycles but then remained highly stable at 91% (AC+100/AC) and 85% (OLC+100/AC) of their initial value, respectively, up to 8000 cycles.

4. CONCLUSIONS

It was demonstrated that ALD allows the deposition of vanadia on free-standing, porous carbon electrodes. Exohedral carbon onions were uniformly coated, while for endohedral AC, micropores were blocked, and the accessible surface area declined extensively at high vanadia loadings. The growth mechanism of vanadia on carbon substrates was characterized by an initial island growth, which began to form a more continuous layer after a sufficient number of ALD cycles. The pore structure proved to have a severe impact on the crystallinity of the resulting vanadia layers. The external surface area of carbon onions provided favorable conditions for crystalline growth, contrarily to the microporous internal surface area of activated carbon, where mostly amorphous vanadia was formed.

The electrochemical performance of the hybrid electrodes was enhanced by the vanadia coating on carbon onions and AC at low specific currents. Yet, only carbon onions as substrate material provided a sufficient electrical conductivity for superior capacity at high rates, while the performance of AC/vanadia electrodes dropped at high charging and discharging rates. Consequently, highly conductive carbons with exohedral surfaces are found to be the superior substrate material for hybrid electrodes. It was found that there is an optimum amount of vanadia that results in an ideal balance between redox-activity and electrical conductivity of the hybrid electrode. In this work, the optimum amount of vanadia was around 50 wt % for activated carbon and 65 wt % for carbon onions. Furthermore, the performance of activated carbon hybrid electrodes dropped drastically due to blocking of internal surface area when exceeding 65 wt % of vanadia. In full-cells, the fabricated carbon/vanadia hybrid electrodes exhibit superior performance only when employed as negative electrodes in an asymmetrical cell.

■ ASSOCIATED CONTENT

Supporting Information

The Supporting Information is available free of charge on the ACS Publications website at DOI: 10.1021/acs.chemmater.6b00738.

TEM of nanodiamond precursor and resulting carbon onions, sedimentation analysis of carbon onions and activated carbon, EFTEM mappings of OLC+100, cross-sectional EDX mappings of all electrodes, XRD of all samples, and galvanostatic charge−discharge profiles of AC+100 during stability testing (PDF)

■ AUTHOR INFORMATION

Corresponding Author

*E-mail: volker.presser@leibniz-inm.de.

Notes

The authors declare no competing financial interest.

■ ACKNOWLEDGMENTS

This work is part of the strategic Leibniz partnership between IPF and INM. We acknowledge funding from the German Federal Ministry for Research and Education (BMBF) in support of the nanoEES^{3D} project (Award No. 03EK3013) as part of the strategic funding initiative energy storage framework. This work is part of the CREATe-Network Project, Horizon 2020 of the European Commission (RISE Project No. 644013). We thank Prof. Arzt (INM) for the continuing support.

■ REFERENCES

(1) Béguin, F.; Presser, V.; Balducci, A.; Frackowiak, E. Carbons and electrolytes for advanced supercapacitors. *Adv. Mater.* **2014**, *26*, 2219−2251.

(2) Simon, P.; Gogotsi, Y. Materials for electrochemical capacitors. *Nat. Mater.* **2008**, *7*, 845−854.

(3) Conway, B. E. *Electrochemical Supercapacitors: Scientific Fundamentals and Technological Applications*; Springer Science & Business Media, 2013.

DOI: 10.1021/acs.chemmater.6b00738
Chem. Mater. 2016, 28, 2802−2813

(4) Qu, D.; Shi, H. Studies of activated carbons used in double-layer capacitors. *J. Power Sources* **1998**, *74*, 99−107.
(5) Shi, H. Activated carbons and double layer capacitance. *Electrochim. Acta* **1996**, *41*, 1633−1639.
(6) Zeiger, M.; Jäckel, N.; Mochalin, V. N.; Presser, V. Review: Carbon onions for electrochemical energy storage. *J. Mater. Chem. A* **2016**, *4*, 3172−3196.
(7) Bushueva, E.; Galkin, P.; Okotrub, A.; Bulusheva, L.; Gavrilov, N.; Kuznetsov, V.; Moiseekov, S. Double layer supercapacitor properties of onion-like carbon materials. *Phys. Status Solidi B* **2008**, *245*, 2296−2299.
(8) Frackowiak, E.; Jurewicz, K.; Delpeux, S.; Beguin, F. Nanotubular materials for supercapacitors. *J. Power Sources* **2001**, *97-98*, 822−825.
(9) Frackowiak, E.; Metenier, K.; Bertagna, V.; Beguin, F. Supercapacitor electrodes from multiwalled carbon nanotubes. *Appl. Phys. Lett.* **2000**, *77*, 2421−2423.
(10) Zhang, L. L.; Zhou, R.; Zhao, X. Graphene-based materials as supercapacitor electrodes. *J. Mater. Chem.* **2010**, *20*, 5983−5992.
(11) Jo, K.; Gu, M.; Kim, B.-S. Ultrathin Supercapacitor Electrode Based on Reduced Graphene Oxide Nanosheets Assembled with Photo-Cross-Linkable Polymer: Conversion of Electrochemical Kinetics in Ultrathin Films. *Chem. Mater.* **2015**, *27*, 7982−7989.
(12) Atchison, J. S.; Zeiger, M.; Tolosa, A.; Funke, L. M.; Jäckel, N.; Presser, V. Electrospinning of ultrafine metal oxide/carbon and metal carbide/carbon nanocomposite fibers. *RSC Adv.* **2015**, *5*, 35683−35692.
(13) Ra, E.; Raymundo-Piñero, E.; Lee, Y.; Béguin, F. High power supercapacitors using polyacrylonitrile-based carbon nanofiber paper. *Carbon* **2009**, *47*, 2984−2992.
(14) Fischer, U.; Saliger, R.; Bock, V.; Petricevic, R.; Fricke, J. Carbon aerogels as electrode material in supercapacitors. *J. Porous Mater.* **1997**, *4*, 281−285.
(15) Lozano-Castello, D.; Cazorla-Amorós, D.; Linares-Solano, A.; Shiraishi, S.; Kurihara, H.; Oya, A. Influence of pore structure and surface chemistry on electric double layer capacitance in non-aqueous electrolyte. *Carbon* **2003**, *41*, 1765−1775.
(16) Marsh, H.; Reinoso, F. R. *Activated Carbon*; Elsevier, 2006.
(17) Pérez, C. R.; Yeon, S. H.; Ségalini, J.; Presser, V.; Taberna, P. L.; Simon, P.; Gogotsi, Y. Structure and Electrochemical Performance of Carbide-Derived Carbon Nanopowders. *Adv. Funct. Mater.* **2013**, *23*, 1081−1089.
(18) Portet, C.; Yushin, G.; Gogotsi, Y. Electrochemical performance of carbon onions, nanodiamonds, carbon black and multiwalled nanotubes in electrical double layer capacitors. *Carbon* **2007**, *45*, 2511−2518.
(19) Kuznetsov, V. L.; Chuvilin, A. L.; Butenko, Y. V.; Mal'kov, I. Y.; Titov, V. M. Onion-like carbon from ultra-disperse diamond. *Chem. Phys. Lett.* **1994**, *222*, 343−348.
(20) Zeiger, M.; Jäckel, N.; Aslan, M.; Weingarth, D.; Presser, V. Understanding structure and porosity of nanodiamond-derived carbon onions. *Carbon* **2015**, *84*, 584−598.
(21) Zeiger, M.; Jäckel, N.; Weingarth, D.; Presser, V. Vacuum or flowing argon: What is the best synthesis atmosphere for nanodiamond-derived carbon onions for supercapacitor electrodes? *Carbon* **2015**, *94*, 507−517.
(22) McDonough, J. K.; Frolov, A. I.; Presser, V.; Niu, J.; Miller, C. H.; Ubieto, T.; Fedorov, M. V.; Gogotsi, Y. Influence of the structure of carbon onions on their electrochemical performance in supercapacitor electrodes. *Carbon* **2012**, *50*, 3298−3309.
(23) Jäckel, N.; Weingarth, D.; Zeiger, M.; Aslan, M.; Grobelsek, I.; Presser, V. Comparison of carbon onions and carbon blacks as conductive additives for carbon supercapacitors in organic electrolytes. *J. Power Sources* **2014**, *272*, 1122−1133.
(24) Makgopa, K.; Ejikeme, P. M.; Jafta, C. J.; Raju, K.; Zeiger, M.; Presser, V.; Ozoemena, K. I. A high-rate aqueous symmetric pseudocapacitor based on highly graphitized onion-like carbon/birnessite-type manganese oxide nanohybrids. *J. Mater. Chem. A* **2015**, *3*, 3480−3490.
(25) Kovalenko, I.; Bucknall, D. G.; Yushin, G. Detonation Nanodiamond and Onion-Like-Carbon-Embedded Polyaniline for Supercapacitors. *Adv. Funct. Mater.* **2010**, *20*, 3979−3986.
(26) Anjos, D. M.; McDonough, J. K.; Perre, E.; Brown, G. M.; Overbury, S. H.; Gogotsi, Y.; Presser, V. Pseudocapacitance and performance stability of quinone-coated carbon onions. *Nano Energy* **2013**, *2*, 702−712.
(27) Zhang, Y.; Feng, H.; Wu, X.; Wang, L.; Zhang, A.; Xia, T.; Dong, H.; Li, X.; Zhang, L. Progress of electrochemical capacitor electrode materials: A review. *Int. J. Hydrogen Energy* **2009**, *34*, 4889−4899.
(28) Simon, P.; Gogotsi, Y.; Dunn, B. Where do batteries end and supercapacitors begin? *Science* **2014**, *343*, 1210−1211.
(29) Rakhi, R.; Ahmed, B.; Hedhili, M.; Anjum, D. H.; Alshareef, H. N. Effect of Postetch Annealing Gas Composition on the Structural and Electrochemical Properties of Ti_2CT_x MXene Electrodes for Supercapacitor Applications. *Chem. Mater.* **2015**, *27*, 5314−5323.
(30) Liu, J.; Essner, J.; Li, J. Hybrid supercapacitor based on coaxially coated manganese oxide on vertically aligned carbon nanofiber arrays. *Chem. Mater.* **2010**, *22*, 5022−5030.
(31) Levi, M. D.; Lukatskaya, M. R.; Sigalov, S.; Beidaghi, M.; Shpigel, N.; Daikhin, L.; Aurbach, D.; Barsoum, M. W.; Gogotsi, Y. Solving the Capacitive Paradox of 2D MXene using Electrochemical Quartz-Crystal Admittance and In Situ Electronic Conductance Measurements. *Adv. Energy Mater.* **2015**, *5*, 1400815.
(32) Zhang, K.; Zhang, L. L.; Zhao, X.; Wu, J. Graphene/polyaniline nanofiber composites as supercapacitor electrodes. *Chem. Mater.* **2010**, *22*, 1392−1401.
(33) Salloux, K.; Chaput, F.; Wong, H.; Dunn, B.; Breiter, M. Lithium intercalation in vanadium pentoxide aerogels. *J. Electrochem. Soc.* **1995**, *142*, L191−L192.
(34) Takahashi, K.; Limmer, S. J.; Wang, Y.; Cao, G. Synthesis and electrochemical properties of single-crystal V_2O_5 nanorod arrays by template-based electrodeposition. *J. Phys. Chem. B* **2004**, *108*, 9795−9800.
(35) Wang, Y.; Takahashi, K.; Lee, K.; Cao, G. Nanostructured vanadium oxide electrodes for enhanced lithium-ion intercalation. *Adv. Funct. Mater.* **2006**, *16*, 1133.
(36) Laheäär, A.; Przygocki, P.; Abbas, Q.; Béguin, F. Appropriate methods for evaluating the efficiency and capacitive behavior of different types of supercapacitors. *Electrochem. Commun.* **2015**, *60*, 21−25.
(37) Brousse, T.; Bélanger, D.; Long, J. W. To be or not to be pseudocapacitive? *J. Electrochem. Soc.* **2015**, *162*, A5185−A5189.
(38) Bandaru, P.; Yamada, H.; Narayanan, R.; Hoefer, M. Charge transfer and storage in nanostructures. *Mater. Sci. Eng., R* **2015**, *96*, 1−69.
(39) Gu, W.; Yushin, G. Review of nanostructured carbon materials for electrochemical capacitor applications: advantages and limitations of activated carbon, carbide-derived carbon, zeolite-templated carbon, carbon aerogels, carbon nanotubes, onion-like carbon, and graphene. *Wiley Interdiscip. Rev.: Energy Environ.* **2014**, *3*, 424−473.
(40) Yilmaz, G.; Guo, C. X.; Lu, X. High Performance Solid-State Supercapacitors Based on V_2O_5/Carbon Nanotube Composites. *ChemElectroChem* **2016**, *3*, 158−164.
(41) Boukhalfa, S.; Evanoff, K.; Yushin, G. Atomic layer deposition of vanadium oxide on carbon nanotubes for high-power supercapacitor electrodes. *Energy Environ. Sci.* **2012**, *5*, 6872−6879.
(42) Chen, Z.; Augustyn, V.; Wen, J.; Zhang, Y.; Shen, M.; Dunn, B.; Lu, Y. High-Performance Supercapacitors Based on Intertwined CNT/V_2O_5 Nanowire Nanocomposites. *Adv. Mater.* **2011**, *23*, 791−795.
(43) Zeiger, M.; Weingarth, D.; Presser, V. Quinone-Decorated Onion-Like Carbon/Carbon Fiber Hybrid Electrodes for High-Rate Supercapacitor Applications. *ChemElectroChem* **2015**, *2*, 1117−1127.
(44) Benson, J.; Boukhalfa, S.; Magasinski, A.; Kvit, A.; Yushin, G. Chemical vapor deposition of aluminum nanowires on metal substrates for electrical energy storage applications. *ACS Nano* **2012**, *6*, 118−125.

DOI: 10.1021/acs.chemmater.6b00738
Chem. Mater. 2016, 28, 2802−2813

(45) Luo, J.; Xia, X.; Luo, Y.; Guan, C.; Liu, J.; Qi, X.; Ng, C. F.; Yu, T.; Zhang, H.; Fan, H. J. Rationally designed hierarchical TiO_2@Fe_2O_3 hollow nanostructures for improved lithium ion storage. *Adv. Energy Mater.* **2013**, *3*, 737−743.
(46) Chen, X.; Pomerantseva, E.; Banerjee, P.; Gregorczyk, K.; Ghodssi, R.; Rubloff, G. Ozone-Based Atomic Layer Deposition of Crystalline V_2O_5 Films for High Performance Electrochemical Energy Storage. *Chem. Mater.* **2012**, *24*, 1255−1261.
(47) Daubert, J. S.; Lewis, N. P.; Gotsch, H. N.; Mundy, J. Z.; Monroe, D. N.; Dickey, E. C.; Losego, M. D.; Parsons, G. N. Effect of Meso-and Micro-Porosity in Carbon Electrodes on Atomic Layer Deposition of Pseudocapacitive V_2O_5 for High Performance Supercapacitors. *Chem. Mater.* **2015**, *27*, 6524−6534.
(48) Azhagan, M. V. K.; Vaishampayan, M. V.; Shelke, M. V. Synthesis and electrochemistry of pseudocapacitive multilayer fullerenes and MnO_2 nanocomposites. *J. Mater. Chem. A* **2014**, *2*, 2152−2159.
(49) George, S. M. Atomic layer deposition: an overview. *Chem. Rev.* **2010**, *110*, 111−131.
(50) Wang, X.; Yushin, G. Chemical vapor deposition and atomic layer deposition for advanced lithium ion batteries and supercapacitors. *Energy Environ. Sci.* **2015**, *8*, 1889−1904.
(51) Jäckel, N.; Weingarth, D.; Schreiber, A.; Krüner, B.; Zeiger, M.; Tolosa, A.; Aslan, M.; Presser, V. Performance evaluation of conductive additives for activated carbon supercapacitors in organic electrolyte. *Electrochim. Acta* **2016**, *191*, 284−298.
(52) Brunauer, S.; Emmett, P. H.; Teller, E. Adsorption of gases in multimolecular layers. *J. Am. Chem. Soc.* **1938**, *60*, 309−319.
(53) Gor, G. Y.; Thommes, M.; Cychosz, K. A.; Neimark, A. V. Quenched solid density functional theory method for characterization of mesoporous carbons by nitrogen adsorption. *Carbon* **2012**, *50*, 1583−1590.
(54) Weingarth, D.; Zeiger, M.; Jäckel, N.; Aslan, M.; Feng, G.; Presser, V. Graphitization as a Universal Tool to Tailor the Potential-Dependent Capacitance of Carbon Supercapacitors. *Adv. Energy Mater.* **2014**, *4*, 1400316.
(55) Ruch, P.; Cericola, D.; Hahn, M.; Kötz, R.; Wokaun, A. On the use of activated carbon as a quasi-reference electrode in non-aqueous electrolyte solutions. *J. Electroanal. Chem.* **2009**, *636*, 128−131.
(56) Kuznetsov, V.; Butenko, Y. V.; Zaikovskii, V.; Chuvilin, A. Carbon redistribution processes in nanocarbons. *Carbon* **2004**, *42*, 1057−1061.
(57) Yanguas-Gil, A.; Libera, J. A.; Elam, J. W. Modulation of the Growth Per Cycle in Atomic Layer Deposition Using Reversible Surface Functionalization. *Chem. Mater.* **2013**, *25*, 4849−4860.
(58) Baddour-Hadjean, R.; Golabkan, V.; Pereira-Ramos, J.; Mantoux, A.; Lincot, D. A Raman study of the lithium insertion process in vanadium pentoxide thin films deposited by atomic layer deposition. *J. Raman Spectrosc.* **2002**, *33*, 631−638.
(59) Lee, S.-H.; Cheong, H. M.; Seong, M. J.; Liu, P.; Tracy, C. E.; Mascarenhas, A.; Pitts, J. R.; Deb, S. K. Raman spectroscopic studies of amorphous vanadium oxide thin films. *Solid State Ionics* **2003**, *165*, 111−116.
(60) Wang, X.; Li, H.; Fei, Y.; Wang, X.; Xiong, Y.; Nie, Y.; Feng, K. XRD and Raman study of vanadium oxide thin films deposited on fused silica substrates by RF magnetron sputtering. *Appl. Surf. Sci.* **2001**, *177*, 8−14.
(61) Julien, C.; Ivanov, I.; Gorenstein, A. Vibrational modifications on lithium intercalation in V_2O_5 films. *Mater. Sci. Eng., B* **1995**, *33*, 168−172.
(62) Ferrari, A. C. *Mater. Res. Soc. Symp. Proc.* **2001**, W11.15.11.
(63) Ferrari, A. C.; Robertson, J. Interpretation of Raman spectra of disordered and amorphous carbon. *Phys. Rev. B: Condens. Matter Mater. Phys.* **2000**, *61*, 14095.
(64) Cebik, J.; McDonough, J. K.; Peerally, F.; Medrano, R.; Neitzel, I.; Gogotsi, Y.; Osswald, S. Raman spectroscopy study of the nanodiamond-to-carbon onion transformation. *Nanotechnology* **2013**, *24*, 205703.
(65) Thommes, M.; Kaneko, K.; Neimark, A. V.; Olivier, J. P.; Rodriguez-Reinoso, F.; Rouquerol, J.; Sing, K. S. Physisorption of gases, with special reference to the evaluation of surface area and pore size distribution (IUPAC Technical Report). *Pure Appl. Chem.* **2015**, *87*, 1051−1069.
(66) Zhang, S.; Pan, N. Supercapacitors performance evaluation. *Adv. Energy Mater.* **2015**, *5*, 1401401.
(67) Xia, J.; Chen, F.; Li, J.; Tao, N. Measurement of the quantum capacitance of graphene. *Nat. Nanotechnol.* **2009**, *4*, 505−509.
(68) Liu, H.; Yang, W. Ultralong single crystalline V_2O_5 nanowire/graphene composite fabricated by a facile green approach and its lithium storage behavior. *Energy Environ. Sci.* **2011**, *4*, 4000−4008.
(69) Coustier, F.; Lee, J.-M.; Passerini, S.; Smyrl, W. H. V_2O_5 aerogel-like lithium intercalation host. *Solid State Ionics* **1999**, *116*, 279−291.
(70) Hu, Y. S.; Liu, X.; Müller, J. O.; Schlögl, R.; Maier, J.; Su, D. S. Synthesis and Electrode Performance of Nanostructured V_2O_5 by Using a Carbon Tube-in-Tube as a Nanoreactor and an Efficient Mixed-Conducting Network. *Angew. Chem., Int. Ed.* **2009**, *48*, 210−214.
(71) Cao, A. M.; Hu, J. S.; Liang, H. P.; Wan, L. J. Self-assembled vanadium pentoxide (V_2O_5) hollow microspheres from nanorods and their application in lithium-Ion batteries. *Angew. Chem., Int. Ed.* **2005**, *44*, 4391−4395.

DOI: 10.1021/acs.chemmater.6b00738
Chem. Mater. 2016, 28, 2802−2813